Journal of Power Sources 219 (2012) 155–162

Contents lists available at SciVerse ScienceDirect

Journal of Power Sources

journal homepage: www.elsevier.com/locate/jpowsour

Preparation and characterization of Ca–Sm–Ce mixed oxides via cellulose templating method for solid oxide fuel cell applications

Hasan Özdemir, Vedat Sarıboğa, M.A. Faruk Öksüzömer*, M. Ali Gürkaynak

Department of Chemical Engineering, Istanbul University, 34320 Avcılar, Istanbul, Turkey

HIGHLIGHTS

- Ca–Sm–Ce mixed oxides were synthesized via cellulose templating method firstly.
- Maximum solubility limit of CaO in CeO_2 was found to be 9.4 mol%.
- It was observed that Sm^{+3} expands the CeO_2 lattice more than Ca^{+2}.
- Conductivity of $Sm_{0.1}Ca_{0.1}Ce_{0.8}O_x$ was found to be 0.032 S cm^{-1} at 800 °C.

GRAPHICAL ABSTRACT

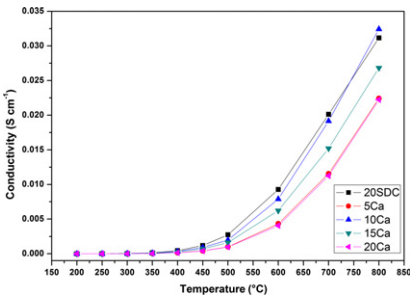

ARTICLE INFO

Article history:
Received 20 April 2012
Received in revised form
3 July 2012
Accepted 13 July 2012
Available online 20 July 2012

Keywords:
Intermediate temperature solid oxide fuel cell
Samarium doped ceria
Calcium doped ceria
CaO solubility
Cellulose templating method
Electrolyte

ABSTRACT

$Sm_xCa_{0.2-x}Ce_{0.8}O_y$ materials are synthesized by changing mol ratios of the composition as $x = 0$, 0.05, 0.1, 0.15 and 0.2, respectively, with a fast and facile cellulose templating method for the first time. Microstructures of the calcined and sintered samples are characterized by XRD and SEM-EDX. Density measurements are actualized by using Archimedes method. The electrical conductivity of the samples is obtained from two-probe impedance spectroscopy. Maximum solubility limit of CaO in CeO_2 is found to be 9.4 mol% from the XRD results. Incorporation of CaO slightly increases the sinterability of the samples. It is observed that Sm^{+3} expands the CeO_2 lattice more than Ca^{+2}. 10 mol% CaO incorporated sample show the highest total conductivity with the value of 0.032 S cm^{-1} at 800 °C. Obtained results show that $Sm_{0.1}Ca_{0.1}Ce_{0.8}O_y$ can be an excellent candidate for intermediate temperature solid oxide fuel cell applications due to its lower cost and higher performance compared to $Sm_{0.2}Ce_{0.8}O_y$ at 800 °C. Additionally, cellulose templating method can be used as an effective method in order to prepare mixed oxide structures since the performances of the samples are higher than the samples which are prepared by more complex or costly hydrothermal and co-precipitation methods in literature.

1. Introduction

Solid oxide fuel cells (SOFCs) can provide efficient and clean energy conversion in a variety of applications ranging from small auxiliary power units to large scale power plants [1]. While the current SOFC technology requires high temperatures (800–1000 °C) due to the usage of high temperature ionic conductive electrolyte materials such as 8 mol % Y_2O_3-stabilized ZrO_2 (8YSZ), is still expensive for SOFC applications. It is necessary to lower the operating temperature so as to minimize chemical instability, lack of flexibility in selection of materials and thermal expansion mismatch between anode–electrolyte or electrolyte–cathode. Thus, intermediate temperature SOFCs (IT-SOFCs) are quite attractive. The key requirement for the IT-SOFC is the electrolyte material which has to

* Corresponding author. Tel.: +90 212 440 00 00x17652.
E-mail address: fufu@istanbul.edu.tr (M.A. Faruk Öksüzömer).

0378-7753/$ – see front matter © 2012 Elsevier B.V. All rights reserved.
http://dx.doi.org/10.1016/j.jpowsour.2012.07.033

be a good ionic conductor to minimize cell impedance, but also shows little or no electronic conduction to minimize leakage currents and stable under operating conditions.

Rare-earth doped ceria $Ce_{1-x}M_xO_y$ (M = Sm, Gd) (known as SDC or GDC) where $x = 0.15–0.20$ have been considered as promising oxide electrolytes for IT-SOFCs due to higher values of ionic conductivity than 8YSZ in the temperature range 500–700 °C [2–4]. However, from the viewpoint of material expenses and stability, both Gd and Sm are very costly and these ceria based electrolytes are not stable under reducing conditions due to the reduction of Ce^{+4} to Ce^{+3} [5,6]. Hence, there is an increasing interest to identify and develop new ceria based oxides using cost-effective dopants for technological applications.

Amongst many alkali or earth alkali oxide dopants, Ca doping not only increases the total conductivity also enhances the stability of the SDC electrolyte. Thus, introduction of CaO into the SDC matrix could be an effective solution as claimed by several authors [7–10].

Therefore, in order to investigate the effect of calcium doping we synthesized $Sm_xCa_{0.2-x}Ce_{0.8}O_y$ materials by changing mol ratios of the composition as $x = 0$, 0.05, 0.1, 0.15 and 0.2, respectively, with a fast and facile cellulose templating method for the first time.

2. Experimental

2.1. Preparation of Ca–Sm–Ce mixed oxides

$Sm_{0.2}Ce_{0.8}O_y$ (20SDC), $Sm_{0.15}Ca_{0.05}Ce_{0.8}O_y$ (5Ca), $Sm_{0.1}Ca_{0.1}Ce_{0.8}O_y$ (10Ca), $Sm_{0.05}Ca_{0.15}Ce_{0.8}O_y$ (15Ca) and $Ca_{0.2}Ce_{0.8}O_y$ (20Ca) were prepared according to the cellulose templating method reported in the literature [11]. Briefly, $Ce(NO_3)_3.6H_2O$ (Sigma–Aldrich, 99%), $Sm(NO_3)_3.6H_2O$ (Sigma–Aldrich, 99.9%) and/or $Ca(NO_3)_2.4H_2O$ (Sigma–Aldrich, >99%) were dissolved in water and 0.35 M solutions were prepared so as to obtain the desired compositions of the final product. The solutions were carefully dropped onto round ashless filter paper with 125 mm diameter and 0.2 mm thickness (Macharey–Nagel, MN 640 de, ≤2 μm) in the ratio of 1 ml liquid per filter paper. Subsequently, without drying, the impregnated filter papers were transferred into a preheated muffle oven (500 °C), waited for 30 min and then calcined at 800 °C for 6 h in air. Remaining pure mixed oxide sheets were grounded by using mortar & pestle. All Ce-based powders were isostatiscally cold-pressed under 200 MPa. Obtained pellets were sintered at 1200 °C for 6 h.

2.2. Characterization of the samples

Room temperature X-ray diffraction patterns of the calcined powders were revealed by using Rigaku D/Max-2200 diffractometer, using a nickel filtered CuK_α ($\lambda = 0.15{,}406$ nm) radiation. The results were taken over the range of 2θ angles from 10° to 90° at a scanning rate of 1° min^{-1}. The average crystallite diameter of the calcined samples was calculated by using the Scherrer method, $d_{Ni}=K\lambda/\beta \cos\theta$, where the constant K was taken as 0.9, β was the FWHM of the (111) plane and θ was the related angle of this plane. The lattice parameters of the samples were determined by Rietveld analysis using the Maud (Materials analysis using diffraction) software [12].

Scanning electron microscopy (SEM-EDX, FEI Quanta FEG-450) was used in order to investigate the microstructure and analyze the surface phase composition of the sintered samples. All of the samples were coated with ultra-thin gold film to prevent electrostatic charge on the surface.

Density measurements of the sintered pellets were achieved by using the Archimedes method. Briefly, dry pellet weight (W_1), beaker weight with a copper wire immersed into ultra high pure water (W_2) and beaker weight with a copper wire and pellet immersed into ultra high pure water (W_3) were determined and the densities of the pellets (d_p) were calculated according to the equation given below:

$$d_p = \rho \times \frac{W_1}{(W_3 - W_2)} \quad (1)$$

where ρ is the density of the water (27 °C) that was filled into the beaker. The theoretical density was calculated using the following

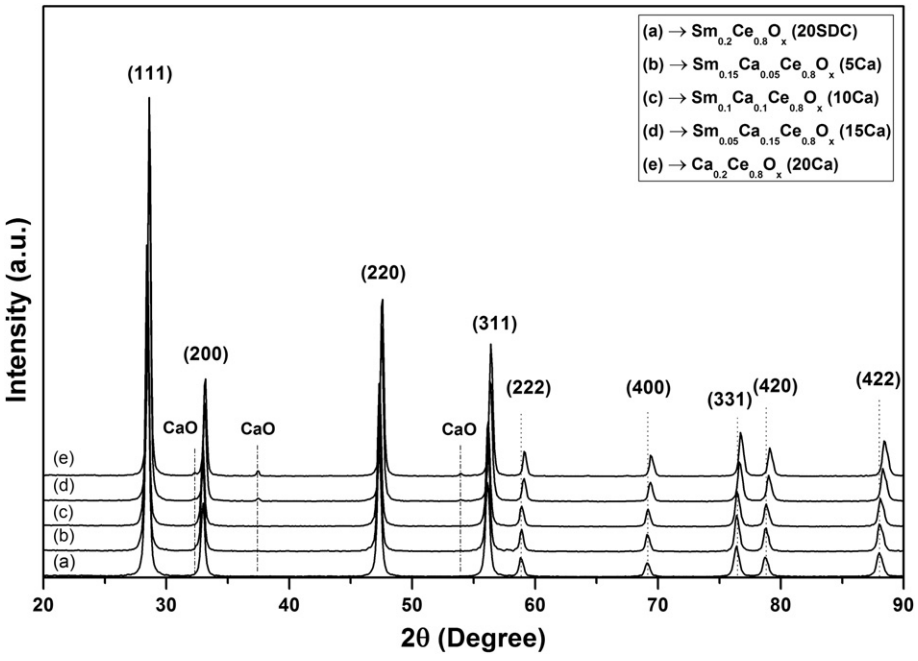

Fig. 1. XRD patterns of the calcined $Sm_xCa_{0.2-x}Ce_{0.8}O_y$ samples.

Table 1
Structural characterization results of the $Sm_xCa_{0.2-x}Ce_{0.8}O_y$ mixed oxide samples.

Composition	Lattice parameter (Å)	Average crystallite size (nm)	Grain size distribution (μm)	Theoretical density (g cm^{-3})	Measured density (g cm^{-3})
$Sm_{0.2}Ce_{0.8}O_x$	5.433 ± 1.86E − 4	24.1	0.6–6	7.15	6.96
$Sm_{0.15}Ca_{0.05}Ce_{0.8}O_x$	5.432 ± 1.4E − 4	28.7	n.d.	6.91	6.75
$Sm_{0.1}Ca_{0.1}Ce_{0.8}O_x$	5.430 ± 1.53E − 4	27.5	0.5–3.2	6.67	6.53
$Sm_{0.05}Ca_{0.15}Ce_{0.8}O_x$	5.412 ± 2.28E − 4	29.8, 33.6[a]	0.53–2.78	6.6	6.52
$Ca_{0.2}Ce_{0.8}O_x$	5.407 ± 2.05E − 4	32, 41.9[a]	0.4–1.91	6.46	6.38

n.d. Grain size couldn't be observed clearly through SEM photographs.
[a] CaO average crystallite size determined from XRD measurements.

equation, considering that Sm^{+3} or Ca^{+2} (to a certain limit which is determined from the XRD results) cations occupy the Ce^{+4} sites to form a solid solution with ceria [13,14]:

$$= 4[(0.8)M_{Ca} + xM_{Sm} + (0.2 - x)M_{Ca} + (1.6 + 1.5x + (0.2 - x))M_0]/a^3N_A \quad (2)$$

where x is the dopant concentration, a is the lattice constant of the solid solution at room temperature, N_A is the Avagadro constant, and M denotes the atomic weight. Additionally, theoretical density was corrected for the samples where CaO did not form solid solution according to Eq. (3) given below:

$$\frac{1}{\rho_m} = \frac{W_1}{\rho_1} + \frac{W_2}{\rho_2} \quad (3)$$

where ρ_m is the theoretical density of the mixture, W_1 and W_2 are the weight fractions, ρ_1 and ρ_2 are the theoretical densities of the CaO and solid solution, respectively. The relative density is the ratio between the measured density and theoretical density.

The electrical conductivity of the samples was obtained from two-probe impedance spectroscopy (Solartron 1260). Silver paste was applied to both sides of the pellets as an electrode by firing at 800 °C for 30 min. Measurements were made every 50 °C or 100 °C interval in air over the temperature range of 200–800 °C in air. The frequency range was 10 MHz–10 mHz with an applied voltage of 20 mV.

3. Results and discussion

3.1. XRD, SEM and density results

XRD patterns of the calcined samples are given in Fig. 1. As could be seen, 20SDC, 5Ca and 10Ca samples show mainly ceria related peaks (JCPDS-081-0792). These peaks are shifted towards higher 2θ values with increasing Ca content. Moreover, these shifting are more apparent for 15Ca and 20Ca samples which show small CaO related peaks (JCPDS-082-1691).

It is known that incorporation of dopants into the ceria lattice result with the change of lattice parameter which cause small

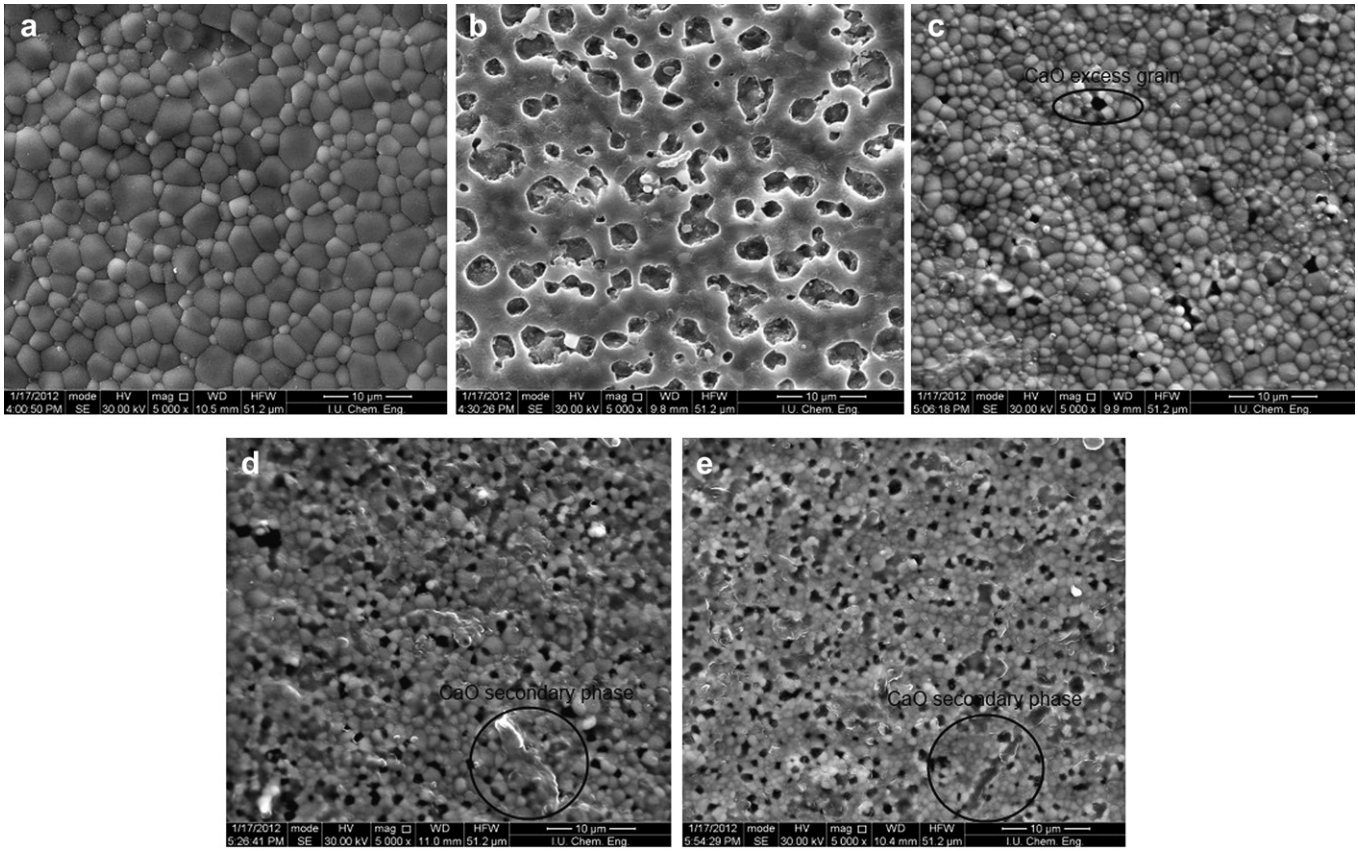

Fig. 2. SEM photographs of the sintered samples at 1200 °C for 6 h a) 20SDC, b) 5Ca, c) 10Ca, d) 15Ca, e) 20Ca.

Table 2
Inner and outer surface phase composition results of the sintered samples determined by SEM-EDX.

Composition	Inner surface (atomic ratios) (%)			Outer surface (atomic ratios) (%)		
	Sm	Ca	Ce	Sm	Ca	Ce
$Sm_{0.2}Ce_{0.8}O_x$	22.14	–	77.86	22.97	–	77.03
$Sm_{0.15}Ca_{0.05}Ce_{0.8}O_x$	15.89	6.08	78.03	11.19	36.36	52.45
$Sm_{0.1}Ca_{0.1}Ce_{0.8}O_x$	11.10	12.28	76.62	11.50	7.16	81.34
$Sm_{0.05}Ca_{0.15}Ce_{0.8}O_x$	6.67	16.22	77.11	6.75	17.86	75.39
$Ca_{0.2}Ce_{0.8}O_x$	–	22.22	77.78	–	20.81	79.19

changes in XRD results [10]. This is due to the differences in ionic radii of Sm^{+3} (1.08 Å), Ca^{+2} (1.12 Å) and Ce^{+4} (0.97 Å) [15] assuming that each ion has a coordination number of 8. Calculated lattice parameters are given in Table 1. The largest lattice parameter is 5.433 Å for 20SDC (and the smallest for the 20Ca) and decreases with the incorporation of Ca^{+2} into the ceria matrix. Normally, it is expected that the lattice parameter might increase due to the incorporation of an ion with a higher ionic radii ($Ca^{+2} > Sm^{+3}$). In our case, the lattice parameter decreases in the reverse order. It's important to note that although we increased the amount of CaO in ceria matrix we also decreased the amount of Sm_2O_3 at the same degree. Therefore, our results imply that the replaced Ca^{+2} ions were not expand the ceria matrix as much as Sm^{+3} ions. Maybe the coordination number of Ca^{+2} is less than 8 therefore the ionic radius is smaller than the theoretical value when they are incorporated with Sm^{+3} into the ceria matrix. Although this situation will remain unclear, there are some results in literature that supports the idea. Dudek [8], found that the lattice parameter of $Ce_{1-x}Sm_xO_2$ material was always higher than the $Ce_{1-x}(Ca_{0.5}Sm_{0.5})_xO_2$ with increase of the x value. Huang et al. [16], prepared Sm or Ca doped ceria materials by hydrothermal method and it was found that the lattice parameters of Sm doped ceria were higher than the Ca doped ceria with the same doping amount. These results strongly suggest that Ca^{+2} could not expand the lattice as much Sm^{+3} ions. Conversely, Banerjee et al. [7] found that the lattice parameter increased to certain extent as they increased the Ca content and decreased the Sm content at the same degree. They also claimed that all Ca formed solid solution with Sm and Ce by interpreting the XRD results. We found that CaO could not dissolve into the ceria matrix after the exact value of 9.4 mol% by using the reference intensity ratio method where I/I_C values determined from the XRD results of 15Ca and 20Ca (containing only Ca as a dopant) samples. In literature, there are many different results about the CaO solubility in ceria matrix. It is reported that the solubility limit is 23 mol% for temperatures in the range of 1450–1650 °C [17], is below than 20 mol% for temperatures lower than 1400 °C [18], is 15 mol% at 1600 °C [19] and little below than the 10 mol% at 1000 °C after kept at that temperature for 40 days [20]. The latter outcome is consisted with our results and implies that the lattice parameter could not increase after 10 mol% CaO incorporation.

Obtained average crystallite diameters are between 27 and 32 nm, which are close to the results obtained with many different complex methods like hydrothermal [16] and co-precipitation [21].

Density results in Table 1 show that the samples are well sintered and their relative densities are higher than 97%. Incorporation

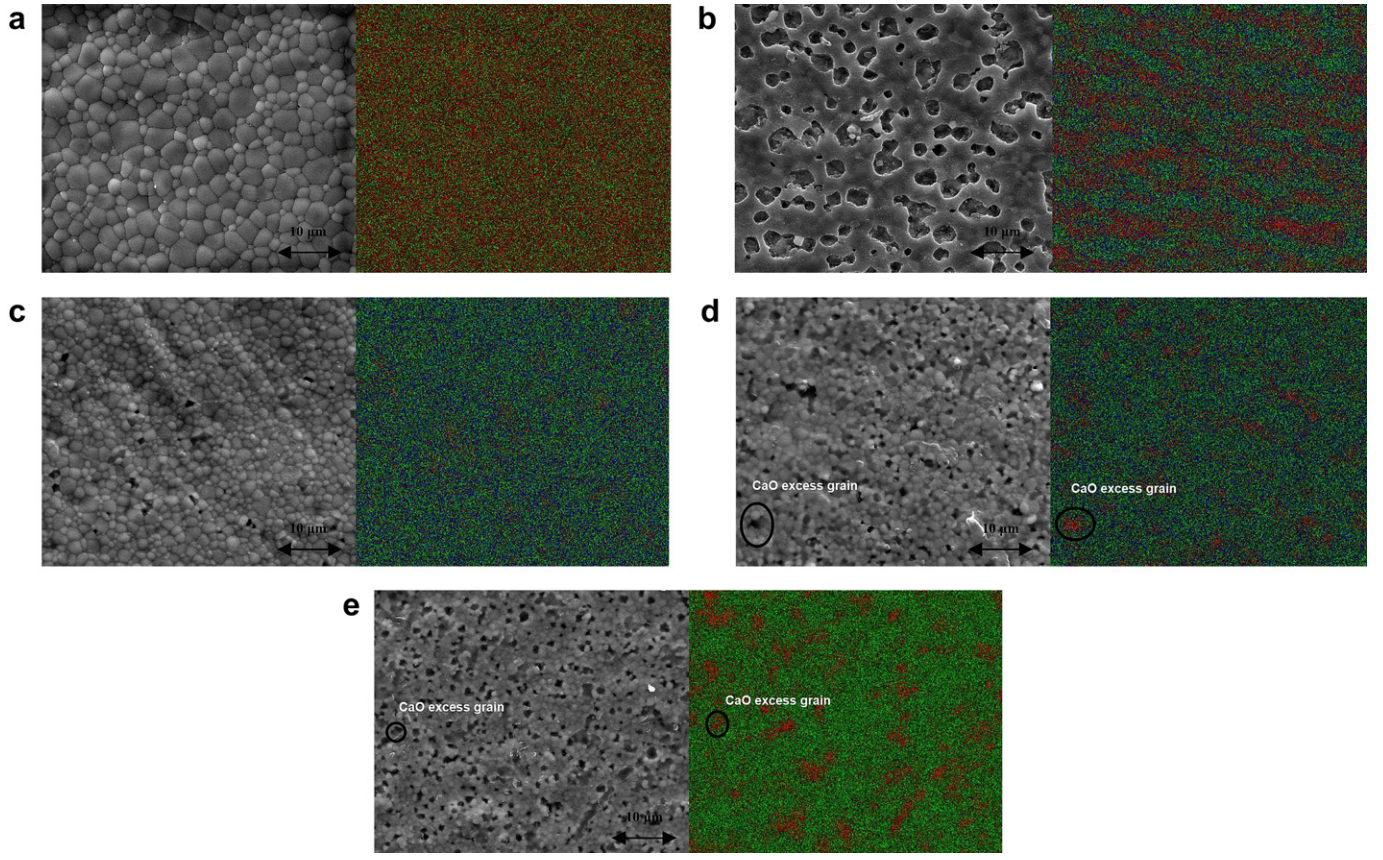

Fig. 3. SEM photographs and related elemental mappings of the sintered samples at 1200 °C for 6 h (green dots – Ce; red dots – Ca; blue dots – Sm: for all samples except 20SDC) a) 20SDC (red dots – Ce; green dots – Sm), b) 5Ca, c) 10Ca, d) 15Ca, e) 20Ca. [For interpretation of color referred in this figure legend, the reader is referred to web version of the article.]

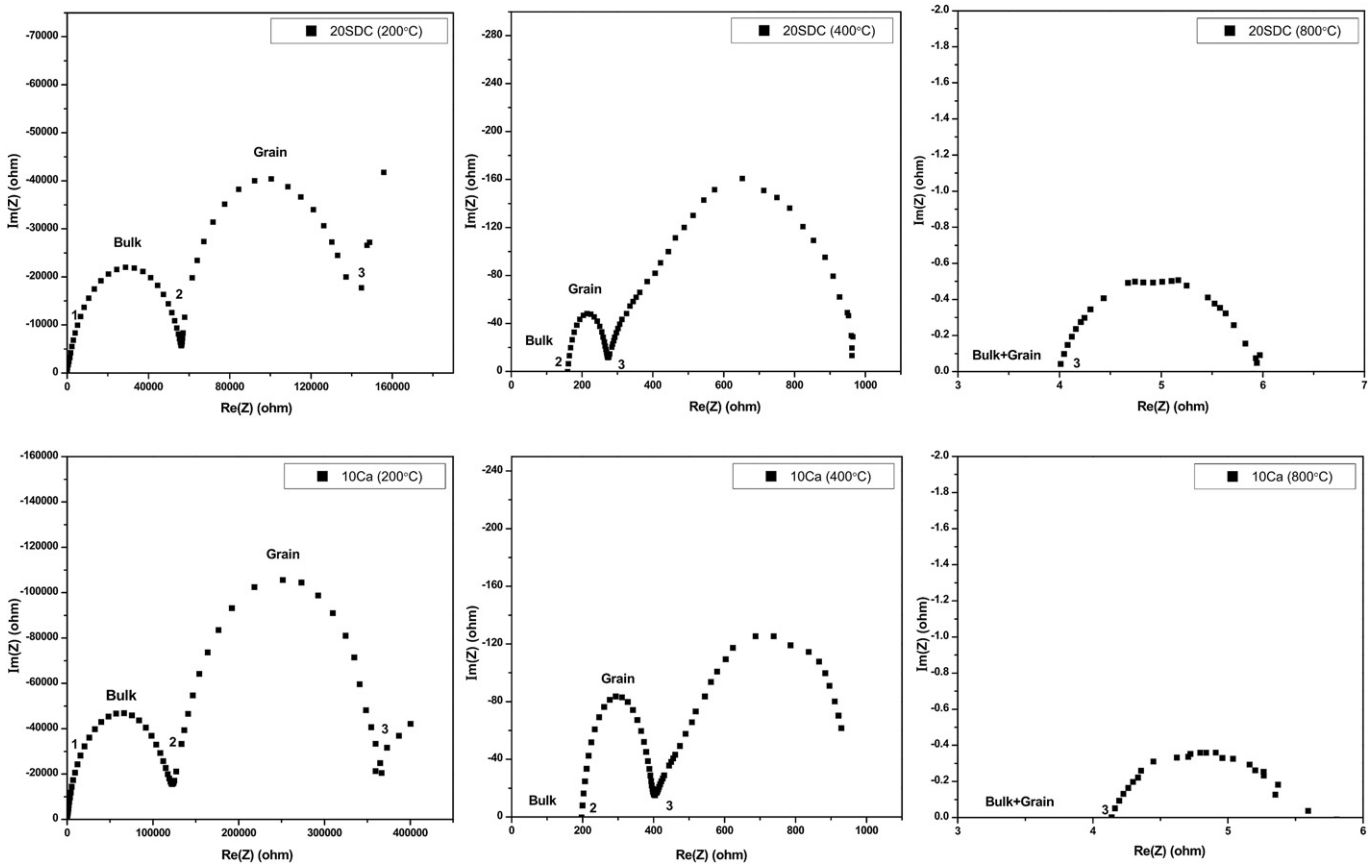

Fig. 4. Nyquist plots of 20SDC and 10Ca samples at different temperatures.

of CaO did not affect the sinterability of the electrolytes negatively, besides slightly improved the sinterability. The required temperature to obtain highly dense electrolytes (>97%) with simple cellulose templating method is 400 °C lower than the conventional solid state method [22] and close to the costly hydrothermal method [7] which shows the effectiveness of this preparation method.

SEM pictures of the outer surfaces of sintered samples are given in Fig. 2. It could be seen that the SDC sample is well sintered. Although, the sinterability of 5Ca sample seems to be the worst amongst others, this conclusion is misleading as could be seen from the density results. Interestingly, CaO segregated on the outer surface of the 5Ca sample and close to the theoretical composition on the inner surface according to the EDX analysis which is given in Table 2. Although we performed the synthesis of the powders and the remaining procedure twice the result was the same which shows there that was no error during synthesis. It could be the result of the preparation method or maybe there is a lower solubility limit for CaO in ceria matrix which could not be detected by XRD analysis although there was no report for such behavior [7] and will be investigated in our next work. 10Ca sample shows more uniform and dense structure. Dark fields represent the CaO excess grains [21] (also could be well seen in Fig. 3d, e) and there is no observable secondary CaO phase. But, it could be seen that both 15Ca and 20Ca samples contain great amounts of CaO excess grains and CaO secondary phases. These results are in accordance with the XRD results as we found the solubility limit of CaO 9.4 mol%.

Additionally, we performed elemental mapping analysis for all samples in order to observe the distribution of the oxides visually. It could be seen that Sm_2O_3 is homogenously dispersed in CeO_2 for 20SDC sample in Fig. 3. Although Sm_2O_3 is well distributed, there are huge clusters of CaO on the outer surface of 5Ca sample. Distribution of both Sm_2O_3 and CaO are uniform on 10Ca sample. But as the CaO amount increased to 15 mol% and 20 mol% clusters of CaO could be observable on 15Ca and 20Ca samples respectively. Insoluble CaO in CeO_2 existed as a second phase and forms small clusters which could be detrimental for ionic conductivity.

Grain size distributions, which are determined from the SEM photos in Fig. 2, are specified in Table 1. It is clear that the size

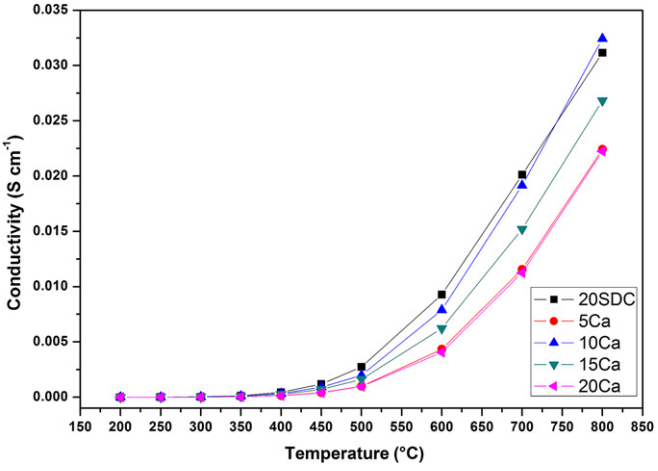

Fig. 5. Conductivity results of the $Sm_xCa_{0.2-x}Ce_{0.8}O_y$ samples.

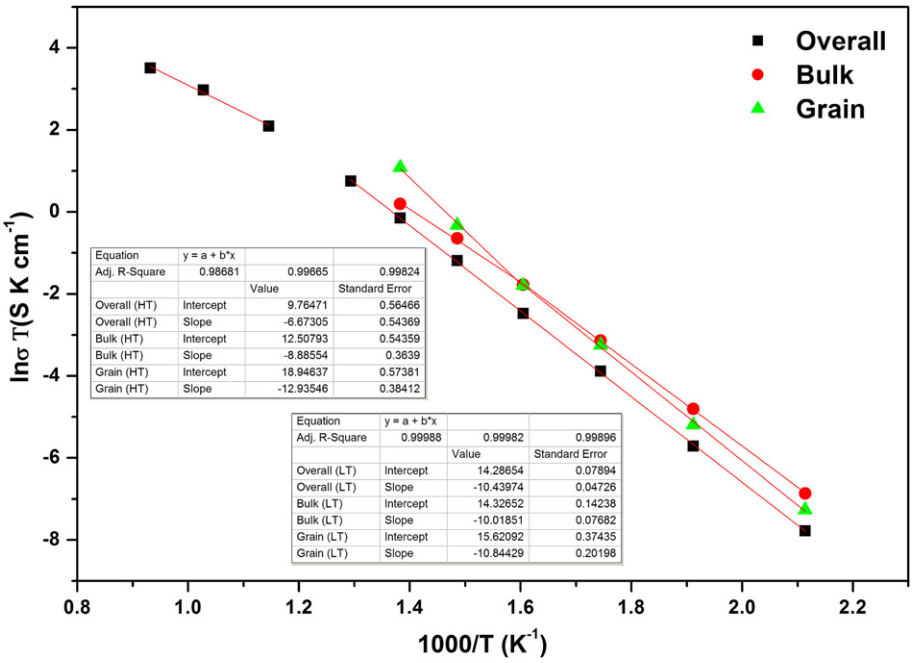

Fig. 6. Arrhenius plot of 20SDC sample.

distribution gets narrower with the increasing of CaO amount where insoluble CaO suppresses the grain growth by blocking the way as they form independent grains for 15Ca and 20Ca samples.

3.2. Impedance results

Impedance spectroscopy is a powerful tool to study the electrical properties of solid electrolytes. In addition to the total ionic conductivity, it is also possible to get the information about the electrode process and in the case of polycrystalline samples, the separate contributions of the bulk and the grain-boundary resistance.

In Fig. 4, typical results obtained from impedance measurements are given. Real component (Re(Z)) plotted against imaginary component (Im(Z)) is called Nyquist plot which is obtained by applying a small sinusoidal voltage across the sample and measuring the amplitude and phase angle (θ) of the current. At low temperatures between 200 and 350 °C, three arcs could be observed in the Nyquist plot. It was found that the capacitance values were in the range usually expected (10^{-11}–10^{-8} F) for resistive grain-boundary processes [23]. The capacitance of the grain-relaxation process is much smaller compared to that of the grain boundary and is typically in the range of picofarads [23]. Hence, we have considered the resistance corresponding to arc (1)

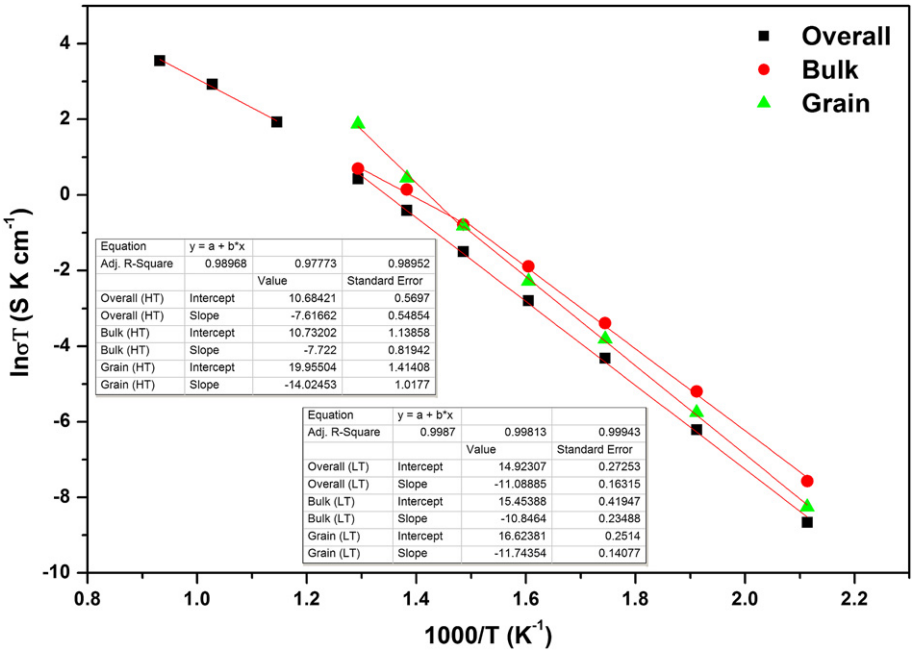

Fig. 7. Arrhenius plot of 10Ca sample.

(see Fig. 4) as the bulk (grain interior or lattice) resistivity, arc (2) as the grain (grain-boundary) resistivity and arc (3) as the electrode resistivity. As the temperature increases, arc (1) corresponding to bulk resistivity disappears and only grain and electrode resistivity are observable (between 400 and 500 °C). Still, bulk resistivity could be calculated by measuring the distance between the vertical axis and the interception point of the impedance semicircle, corresponding to the grain with the horizontal axis. After 500 °C, only the semicircle corresponding to electrode remains and it is impossible to determine the bulk or grain resistivity separately. Therefore, only the total resistivity could be calculated at higher temperatures than 500 °C.

Total conductivity of the samples is given in Fig. 5 calculated by Eq. (4):

$$\sigma_{\text{overall}} = \frac{1}{R_{\text{overall}}} \times \frac{l}{A} \quad (4)$$

where R_{overall} is the sum of bulk and grain resistance, l is the thickness of the electrolyte and A is the area of the electrodes.

Total conductivity of the samples decrease according to the 20SDC > 10Ca > 15Ca > 5Ca > 20Ca sequence between 200 °C and 700 °C. But at 800 °C, this sequence is changed and 10Ca sample show the highest conductivity with the value of 0.032 S cm^{-1} which is higher than the 20SDC (0.031 S cm^{-1}). Although the CaO content of 5Ca sample is lower than the other Ca included samples and its conductivity was expected to be between 20SDC and 10Ca, the conductivity is poor and close to the 20Ca sample due to the external surface of the sample has much more CaO than the expected value which lowers the conductivity of the sample.

Despite the 20Ca sample give the lowest conductivity value (4×10^{-3} S cm^{-1}) at 600 °C, it is much higher than the value (4.2×10^{-4} S cm^{-1}) of the sample prepared by hydrothermal method with approximate compositions and higher sintering temperature (1400–1450 °C for 6 h) in literature [16]. In case of 20SDC the obtained value (9.3×10^{-3} S cm^{-1}) is very close to the value (approx. 1×10^{-2} S cm^{-1}) obtained from another work by using solid state reaction and sintering at 1640 °C for 6 h [22]. These results show that cellulose templating method is an effective method to produce ionic conductive mixed oxides less costly and without giving much effort.

Arrhenius plots (according to the equation: $\ln \sigma T = \ln \sigma_0 - E_a/kT$) of the 20SDC and 10Ca samples are given in Figs. 6 and 7, respectively. The other figures are not given for brevity and instead, all the results are presented in Table 3. In the figures, logarithmic overall, bulk and grain conductivity multiplied by temperature are plotted against the inverse of temperature as K^{-1}. According to the results, there are two parts called as LT (low temperature regime) and HT (high temperature regime) where the linearity of the plots change and thus the activation energy of the bulk, grain and overall conductivity change with increasing temperature. Although bulk and grain conductivity could be observable up to 500 °C, the change of the activation energy begins at nearly 400 °C and thus could be calculated for the higher temperature regime.

It has been shown that oxygen ionic conductivity in rare-earth (Re^{+3})-doped ceria can be represented by the following equations [24];

$$\text{at low temperatures} \quad \sigma = \frac{\sigma_0}{T} e^{-\left(\frac{\Delta H_m - \Delta H_a}{kT}\right)} \quad (5)$$

$$\text{at high temperatures} \quad \sigma = \frac{\sigma_0}{T} e^{-\left(\frac{\Delta H_m}{kT}\right)} \quad (6)$$

where ΔH_m is the migration enthalpy of the oxygen ions and ΔH_a is the association enthalpy of the dopant ion with the oxygen vacancies. Thus the activation energy for conduction becomes the sum of activation energy for migration and association ($E = E_m + E_a$). Generally, it was suggested that at higher temperatures dopant-oxygen vacancy complex dissociates completely to free dopant cation and oxygen vacancy. The concentration of oxygen vacancy is independent of the temperature and equals to the total concentration of dopant cation. Therefore, the migration enthalpy (E_m) could be estimated from the slope of Arrhenius plots in the higher temperature regime. The association enthalpy (E_a) could be calculated from the differences of the slopes at higher and lower temperature regime [25]. According to this, the sample having the lowest migration enthalpy and the highest association enthalpy would have the highest conductivity. As could be seen from Fig. 6 and Table 3, there is a strong relationship between the conductivity and the association enthalpy of the samples. As the 20SDC and 10Ca show approximate conductivity values, their association enthalpy values differ slightly. The correlation with conductivity and association enthalpy follows the same order for the other samples. Also, it seems that the bulk conductivity is dominant at higher temperatures as the overall activation energy values are partially close to bulk activation energy values. Only 20SDC is an exception and it is most likely that the disappearance of the bulk resistivity at 500 °C led to the miscalculation of the activation energy of bulk conductivity at higher temperatures. Therefore, it could be said that the grain size distribution or grain size has a little effect on the performance of the samaria or calcia doped ceria samples as long as the density of the samples are high. The most important part is the bulk composition, and it seems 9.4 mol% CaO, which is the solubility limit in ceria (determined from the XRD results), is the optimum value for co-doping with Sm_2O_3. Thus, it could be possible to obtain less costly and more stable ceria based electrolytes with close performance to $Sm_{0.2}Ce_{0.8}O_y$.

Table 3
Calculated activation energies of $Sm_xCa_{0.2-x}Ce_{0.8}O_y$ mixed oxide samples.

Composition	E (bulk) (eV)		E (grain) (eV)		E (overall) (eV)		
	LT	HT	LT	HT	LT	HT	E_a
$Sm_{0.2}Ce_{0.8}O_x$	0.86	0.77	0.94	1.12	0.9	0.58	0.32
$Sm_{0.15}Ca_{0.05}Ce_{0.8}O_x$	0.93	0.76	0.98	1.07	0.95	0.82	0.13
$Sm_{0.1}Ca_{0.1}Ce_{0.8}O_x$	0.94	0.67	1.01	1.21	0.96	0.66	0.3
$Sm_{0.05}Ca_{0.15}Ce_{0.8}O_x$	0.86	0.64	0.97	1.22	0.92	0.75	0.17
$Ca_{0.2}Ce_{0.8}O_x$	0.94	0.73	1.03	1.03	0.98	0.83	0.15

LT: low temperature regime (200–500 °C) HT: high temperature regime (500–800 °C).

4. Conclusions

$Sm_xCa_{0.2-x}Ce_{0.8}O_y$ materials were synthesized by changing the mol ratios of the composition as x = 0, 0.05, 0.1, 0.15 and 0.2, respectively, with a fast and facile cellulose templating method for the first time. It was found that the CaO incorporation into the CeO_2 matrix is not expanding the lattice as much as Sm_2O_3. Maximum solubility limit of CaO in CeO_2 was found to be 9.4 mol% from the XRD results. Relative densities of the samples were found to be 97% at 1200 °C for 6 h. Incorporation of CaO slightly increases the sinterability of the samples. $Sm_{0.1}Ca_{0.1}Ce_{0.8}O_y$ sample gave the highest conductivity value of 0.032 S cm^{-1} at 800 °C. Impedance results indicate that bulk conductivity is the dominant process at higher temperatures and there is a strong relationship between the association enthalpy and the conductivity of the samples. The cellulose templating method could be used as an effective method in order to prepare mixed oxide structures since the performances of the samples are higher than the samples which were prepared by

more complex or costly hydrothermal and requires much lower sintering temperature compared to solid state reaction method.

Acknowledgement

This study was supported by Istanbul University through project DPT-2008K 121000 and by Istanbul University Research Fund through project no: 3642 and 13207.

References

[1] J.W. Fergus, Journal of Power Sources 162 (2006) 30–40.
[2] R. Mukundan, E. Brosha, D. Brown, F. Garzon, Electrochemical Solid State Letters 2 (1999) 412–414.
[3] S. Zha, C. Xia, G. Meng, Journal of Power Sources 115 (2003) 44–48.
[4] T. Karaca, T.G. Altınçekiç, M.F. Öksüzömer, Ceramics International 36 (2010) 1101–1107.
[5] J.C.C. Abrantes, D. Perez-Coll, P. Nunez, J.R. Frade, Electrochimica Acta 48 (2003) 2761–2766.
[6] Y. Xiong, K. Yamaji, T. Horita, N. Sakai, H. Yokokawa, Journal of the Electrochemical Society 149 (1) (2002) 450–454.
[7] S. Banerjee, P.S. Devi, D. Topwal, S. Mandal, K. Menon, Advanced Functional Materials 17 (2007) 2847–2854.
[8] M. Dudek, Journal of the European Ceramic Society 28 (2008) 965–971.
[9] R. Raza, X. Wang, Y. Ma, B. Zhu, Journal of Power Sources 195 (2010) 6491–6495.
[10] S. Ramesh, V.P. Kumar, P. Kistaiah, C.V. Reddy, Solid State Ionics 181 (2010) 86–91.
[11] K. Langfeld, R. Marschner, B. Frank, R. Schomaker, ChemCatChem 3 (2011) 1354–1358.
[12] http://www.ing.unitn.it/∼maud/.
[13] T. Kudo, H. Obayashi, Journal of the Electrochemical Society 122 (1) (1975) 142–147.
[14] K. Higashi, K. Sonoda, H. Ono, S. Sameshima, Y. Hirata, Journal of Materials Research 14 (1999) 957–967.
[15] R.D. Shannon, Acta Crystallography A32 (1976) 751.
[16] W. Huang, P. Shuk, M. Greenblatt, Chemistry of Materials 9 (1997) 2240–2245.
[17] K. Eguchi, T. Setoguchi, T. Inoue, H. Arai, Solid State Ionics 52 (1992) 165.
[18] M. Yan, T. Mori, J. Zou, F. Ye, D.R. Ou, J. Drennan, Acta Materialia 57 (2009) 722–731.
[19] E.K. Keler, N.A. Godina, A.M. Kalinina, Russian Journal of Inorganic Chemistry 1 (1956) 2557.
[20] B. Zachau-Christiansen, T. Jacobsen, S. Skaarup, Solid State Ionics 86–88 (1996) 725.
[21] M. Yan, T. Mori, F. Ye, D.R. Ou, J. Zou, J. Drennan, Journal of the European Ceramic Society 28 (2008) 2709–2716.
[22] Z. Zhan, T.-L. Wen, H. Tu, Z.-Y. Lu, Journal of the Electrochemical Society 148 (5) (2001) 427–432.
[23] J.T.S. Irvine, D.C. Sinclair, A.R. West, Advanced Materials 2 (1990) 132.
[24] J.A. Kilner, B.C.H. Steele, in: O.T. Sorensen (Ed.), Nonstoichiometric Oxides, Academic Press, London, 1981, p. 233.
[25] S.C. Singhal, K. Kendall, High Temperature Solid Oxide Fuel Cells: Fundamentals, Design, and Applications, Elsevier, Oxford, 2003.